Green's-function approach to nonresonance multiphoton absorption in the alkali-metal atoms

E. J. McGuire
Sandia National Laboratories, Albuquerque, New Mexico 87185
(Received 14 March 1980)

An exact Green's function is constructed for the one-electron Schrödinger equation using a central potential obtained from a piecewise linear approximation to $-rV(r)$ of Herman and Skillman. With the Green's function two- and three-photon ionization cross sections are calculated for He$(1s)(2s)$ ^1S, ^3S, and the alkali metals, and compared to other calculations and experiments. Resonances in the cross sections occur at model eigenvalues rather than experimental energy levels. It is demonstrated that the resonances can be made to occur at experimental values either by simple shifts in the wavelength scale, by adjusting the ionization energy in the calculation, or by including the eigenvalue differences in a finite sum. However, as these are perturbation-theory calculations and not applicable at very high intensities or on resonance, only the wings of the resonance structure are included in the calculation.

I. INTRODUCTION

Theory and experiment on multiphoton absorption in atoms appears to be following the historical pattern of single-photon absorption. Experimentally, the early measurements[1,2] are at discrete wavelengths on the noble gases and alkali metals, but as technology develops continuous sources become available.[3,4] Theoretically, hydrogenic calculations are done early,[5,6] followed by the quantum-defect-method (QDM) calculations.[7,8] The QDM calculations, being semiempirical, are remarkably accurate when the assumptions underlying the method are satisfied. Later, when numerical calculations on single-photon absorption with a one-electron model become available,[9,10] good agreement with measurements on low-Z materials was found, disagreements were found at higher Z, and even more sophisticated calculations were performed.[11,12] The method and calculations reported here for two- and three-photon absorption are numerical calculations with a one-electron model.

In single-photon absorption one calculates the matrix element $\langle i|\vec{r}|f\rangle$, whereas in n-photon absorption the matrix element is

$$M_n=\sum_{1,2,\ldots,n-1}\frac{\langle i|\vec{r}|1\rangle\langle 1|\vec{r}|2\rangle\cdots\langle n-1|\vec{r}|f\rangle}{(E_i-E_1-\omega)(E_i-E_2-2\omega)\cdots[E_i-E_{n-1}-(n-1)\omega]}\,,$$

where $1, 2, \ldots, n-1$ indicate a complete set of atomic states.[6,13,14] One may evaluate M_N by truncating the sums, but there will be a truncation error. To compare calculations with measurements obtained with continuously tunable dye lasers requires calculations over a range of ω, and each portion of the range may require a tedious truncation analysis. Zon *et al.*[8] have pointed out that the sum over one-electron matrix elements of the form $\Sigma_j|j\rangle\langle j|/(\lambda-E_j)$ is the eigenfunction expansion of the one-electron Green's function for the Schrödinger equation. Further, if the Green's function can be written in a characteristic form, i.e.,

$$\sum_j\frac{|j\rangle\langle j|}{(\lambda-E_j)}\rightarrow\mathcal{G}_1(r_<,\lambda)\mathcal{G}_2(r_>,\lambda)\,,$$

then the infinite sum over j is eliminated from the calculation when the characteristic Green's function representation is substituted for the eigenfunction expansion representation. The characteristic Green's function is known for the hydrogenic atom,[15] and, for the general atom, a quantum-defect-method approximation can be developed at large r.[8] When the multiphoton absorption matrix element depends principally on the large portion of the integrands, the QDM Green's function should provide adequate estimates. But, as with the truncated sum, one may have to verify that at each ω the matrix element does depend principally on the large-r integrand.

The technique developed in Sec. II uses an approximate atomic central potential for which an exact Green's function can be written. For a central potential I approximate the quantity $Z(r)=-rV(r)$ of Herman and Skillman[16] by a series of straight lines. The Schrödinger equation is then exactly solvable, for both discrete and continuum orbitals, in terms of Whittaker functions.[17] The model was developed originally[10] to permit the rapid generation of realistic atomic continuum orbitals. The model has been applied to photoionization calculations,[10] Born approximation electron-and proton-ionization rates and stopping

powers, and Auger transition rates,[18] all of which exploit the model's capability of rapidly generating continuum orbitals. But since the solution to the model involves known special functions an exact characteristic Green's function can be written (Sec. II).

The advantage to this approach is that it can be used whenever the multiphoton matrix element can be structured in terms of one-electron Green's functions, and requires no further assumption as to the validity of the QDM approach. It can be used for inner-shell multiphoton absorption and/or for multiphoton absorption from partially filled outer shells. The disadvantage of the approach, a disadvantage inherent in any one electron model, is that the bound-state level structure differs from experiment, and resonances in the multiphoton absorption cross section will appear at the wrong wavelength. This is particularly true for resonances involving low-lying bound levels.

There are several ways of adjusting the model calculations to produce resonances at the experimental energies. First, if the resonances are isolated and the wavelength difference is not large, one can adjust the wavelength scale near the resonance, bringing the resonance position into agreement with experiment. Second, one can change the initial-state ionization energy to produce a resonance at the experimental position. Third, if for only a finite number of levels is there a significant difference between model and experimental eigenvalues, one has

$$\sum_j \frac{|j\rangle\langle j|}{(\lambda - E_j)} = \sum_j \frac{|j\rangle\langle j|}{(\lambda - E_j^0)} + \sum_{j=1} |j\rangle\langle j| \left(\frac{1}{(\lambda - E_j)} - \frac{1}{(\lambda - E_j^0)} \right)$$

$$= \mathcal{G}_1(r_<,)\mathcal{G}_2(r_>, \lambda) + \sum_{j=1}^{N} |j\rangle\langle j| \frac{(E_j - E_j^0)}{(\lambda - E_j)(\lambda - E_j^0)},$$

where $E_j(E_j^0)$ are the experimental (model) eigenvalues. All three approaches will be illustrated in later sections.

In all the calculations reported here the experimental ionization energy is used, and spin-orbit splitting is neglected as near-resonance effects are neglected. A careful discussion of range of validity of the perturbation theory has been given by Beers and Armstrong.[19]

In Sec. II the Green's function is developed. In Secs. III–VIII the calculated two- and three-photon absorption cross sections of He, Li, Na, K, Rb, and Cs are presented and compared with other calculations, and where possible with experiment.

II. GREEN'S-FUNCTION AND CROSS-SECTION EXPRESSIONS

From the discussion in the introduction it is clear that the Green's function has dimension 1/energy. Thus, if $G(\mathrm{Ry})$ is the Green's function in rydbergs and $G(H)$ is the Green's function in hartrees, then $G(H) = 2G(\mathrm{Ry})$. In rydbergs and Bohr radii the Green's function for the Schrödinger equation with a spherically symmetric central potential is

$$[\nabla^2 - V(r) + E]G(\vec{r}, \vec{r}', E) = \delta(\vec{r} - \vec{r}'). \tag{1}$$

If hartree units are used the delta function is multiplied by two.[8] Since

$$\delta(\vec{r} - \vec{r}') = \frac{1}{r^2}\,\delta(r - r') \sum_{l=0}^{\infty} \sum_{m=-l}^{l} Y_{l,m}^*(\theta', \varphi') Y_{lm}(\theta, \varphi), \tag{2}$$

a trial solution of the form

$$G(\vec{r}, \vec{r}', E) = \sum_{l=0}^{\infty} \sum_{m=-l}^{l} g_l(r, r', E) Y_{lm}^*(\theta', \varphi') Y_{lm}(\theta, \varphi) \tag{3}$$

leads to

$$\frac{1}{r}\frac{d^2}{dr^2}[r g_l(r, r', E)] - l\frac{(l+1)}{r^2} g_l(r, r') - [V(r) - E] g_l(r, r') = \frac{1}{r^2}\,\delta(r - r'). \tag{4}$$

With $g_l(r, r') = h_l(r, r')/r$, Eq. (4) becomes

$$\frac{d^2}{dr^2}[h_l(r, r')] - l\frac{(l+1)}{r^2} h_l(r, r') - [V(r) - E] h_l(r, r') = \frac{1}{r}\,\delta(r - r'). \tag{5}$$

For a central potential of the form

$$V(r) = -2Z_i/r + \Delta_i, \quad r_{i-1} \le r \le r_i,$$

with

$$-2Z_i/r_i + \Delta_i = -2Z_{i+1}/r_i + \Delta_{i+1},$$
$$r_0 = 0, \quad \Delta_N = 0, \quad Z_1 = Z_{\text{nucleus}},$$

and with

$$\alpha_i = Z_i/(\Delta_i - E)^{1/2}, \quad E < \Delta_i$$
$$= iZ_i/(E - \Delta_i)^{1/2}, \quad E \ge \Delta_i \tag{6}$$

the homogeneous Schrödinger equation for $h_l(rr', E)$ is solved by a linear combination of Whittaker funtions $M_{\alpha_i, l+1/2}(2rZ_i/\alpha_i)$ and $W_{\alpha_i, l+1/2}(2rZ_i/\alpha_i)$.[10] The Green's function is then determined by standard techniques,[20] and is

$$g_l(r,r',E)=+\frac{1}{(r_<)(r_>)}\left[-\frac{\alpha_1}{2Z_1}\frac{1}{g_{1,2}}\frac{\Gamma(l+1-\alpha_1)}{\Gamma(2l+2)}\right]\left[f_{i,1}M_{\alpha_i,l+1/2}\left(2r_<\frac{Z_i}{\alpha_i}\right)+f_{i,2}W_{\alpha_i,l+1/2}\left(2r_<\frac{Z_i}{\alpha_i}\right)\right]$$
$$\times\left[g_{j,1}M_{\alpha_j,l+1/2}\left(2r_>\frac{Z_j}{\alpha_j}\right)+g_{j,2}W_{\alpha_j,l+1/2}\left(\frac{2r_>}{\alpha_j}Z_j\right)\right]. \tag{7}$$

The inner function satisfies the boundary condition at $r=0$ with

$$f_{i+1,1}=\left(\frac{\alpha_{i+1}}{2Z_{i+1}}\right)\frac{\Gamma(l+1-\alpha_{i+1})}{\Gamma(2l+2)}f_{i,1}[W\alpha_{i+1},M\alpha_i]+f_{i,2}[W\alpha_{i+1},W_{\alpha_i}]),$$
$$f_{i+1,2}=\left(\frac{\alpha_{i+1}}{2Z_{i+1}}\right)\frac{\Gamma(l+1-\alpha_{i+1})}{\Gamma(2l+2)}(f_{i,1}[M_{\alpha_i},M_{\alpha_{i+1}}]+f_{i,2}[W_{\alpha_i},M_{\alpha_{i+1}}]), \tag{8}$$

with $f_{1,1}=1$, $f_{1,2}=0$. The terms in brackets are modified Wronskians, i.e.,

$$[W_{\alpha_i},M_{\alpha_{i+1}}]=W_{\alpha_i,l+1/2}\left(\frac{2rZ_i}{\alpha_i}\right)\frac{d}{dr}M\alpha_{i+1,l+1/2}\left(2r\frac{Z_{i+1}}{\alpha_{i+1}}\right)-M_{\alpha_{i+1},l+1/2}\left(2r\frac{Z_{i+1}}{\alpha_{i+1}}\right)\frac{d}{dr}W_{\alpha_i,l+1/2}\left(2r\frac{Z_i}{\alpha_i}\right). \tag{9}$$

The outer solution depends on the choice of boundary conditions at large r. The recursion relations are

$$g_{i,2}=\frac{\alpha_i}{2Z_i}\frac{\Gamma(l+1-\alpha_i)}{\Gamma(2l+2)}(g_{i+1,1}[W_{\alpha_i},M_{\alpha_{i+1}}]+g_{i+1,2}[W_{\alpha_i},W_{\alpha_{i+1}}]),$$
$$g_{i,2}=\frac{\alpha_i}{2Z_i}\frac{\Gamma(l+1-\alpha_i)}{\Gamma(2l+2)}(g_{i+1,1}[M_{\alpha_{i+1}},M_{\alpha_i}]+g_{i+1,2}[W_{\alpha_{i+1}},M_{\alpha_i}]), \tag{10}$$

with $g_{N,2}=1$ and

$$g_{N,1}=\begin{cases}0, & \text{discrete levels},\\ 0, & \text{incoming waves},\\ (-1)^l\dfrac{\Gamma(l+1+i\alpha_N)}{\Gamma(2l+2)}e^{\pi\alpha_N}, & \text{outgoing waves}.\end{cases} \tag{11}$$

The choice of $g_{N,1}$ for incoming and outgoing waves is a consequence of the choice of $W_{\alpha,l+1/2}(2rZ/\alpha)$, rather than $W_{-\alpha,l+1/2}(-2rZ/\alpha)$ as the second Whittaker function. The quantity S_1 in Eq. (7),

$$S_1=-(\alpha_1/2Z_1)\Gamma(l+1-\alpha_1)/[g_{1,2}\Gamma(2l+2)],$$

is

$$S_j=-(\alpha_j/2Z_j)\Gamma(l+1-\alpha_j)/[\Gamma(2l+2)(f_{j,1}g_{j,2}-g_{j,1}f_{j,2})], \tag{12}$$

evaluated at $j=1$. S_j is independent of j and arises from multiplying Eq. (4) by rdr and integrating between $r'-\epsilon$ and $r'+\epsilon$. With $S_j=S$ the integral is

$$\frac{d}{dr}[rg_l(r,r',E)]|_{r=r'+\epsilon}-\frac{d}{dr}[rg_l(r,r',E)]|_{r=r'-\epsilon}=\frac{1}{r}, \tag{13a}$$

or

$$\frac{S}{r}\left[(f_{j,1}M_{\alpha j}+f_{j,2}W_{\alpha_j})\left(g_{j,1}\frac{dM_{\alpha j}}{dr}+g_{j,2}\frac{dW_{\alpha j}}{dr}\right)-\left(f_{j,1}\frac{dM_{\alpha j}}{dr}+f_{j,2}\frac{dW_{\alpha j}}{dr}\right)(g_{j,1}M_{\alpha j}+g_{j,2}W_{\alpha j})\right]=1/r, \tag{13b}$$

or

$$S\{f_{j,1}g_{j,1}[M_{\alpha j},M_{\alpha j}]+f_{j,2}[W_{\alpha j},W_{\alpha j}]+(f_{j,1}g_{j,2}-f_{j,2}g_{j,1})[M_{\alpha j},W_{\alpha j}]\}=1. \tag{13c}$$

The first two modified Wronskians vanish identically and

$$[M_{\alpha j},W_{\alpha j}]=(2Z_j/\alpha_j)W(M_{\alpha j},W_{\alpha j})=-(2Z_j/\alpha_j)\Gamma(2l+2)/\Gamma(l+1-\alpha_j), \tag{13d}$$

where $W(M_\alpha,W_\alpha)$ is the Wronskian.[17] Thus

$$S=-(\alpha_j/2Z_j)\Gamma(l+1-\alpha_j)/[\Gamma(2l+2)(f_{j,1}g_{j,2}-f_{j,2}g_{j,1})]. \tag{13e}$$

That is, once we choose a sign as $r\to0$ for the inner portion of the Green's function, Eq. (7) fixes the overall sign of the Green's function. The sign used by Zon *et al.*[8] changes from paper to paper.

One can evaluate S at $j=N$, and using $\nu=\alpha_N$, one can write the Green's function for r, $r'>r_{N-1}$ in a

neutral atom ($Z_N = 1$) as

$$g(r,r',E) = -\frac{1}{(r_<)(r_>)}\,\frac{\nu}{2}\,\frac{\Gamma(l+1-\nu)}{\Gamma(2l+2)}\left[M_{\nu,l+1/2}\left(\frac{2r_<}{\nu}\right)+\frac{f_{N,2}}{f_{N,1}}\,W_{\nu,l+1/2}\left(\frac{2r_<}{\nu}\right)\right]W_{\nu,l+1/2}\left(\frac{2r_>}{\nu}\right), \tag{14}$$

where $\nu = \sqrt{-1/E}$ and E is negative for bound states.

To show the relationship of Eq. (14) to the QDM Green's function, we use the Hartree[21] decomposition of the Whittaker functions, i.e.,

$$\begin{aligned} M_{\nu,l+1/2}\left(\frac{2r}{\nu}\right) &= \Gamma(2l+2)G_l\left(2r,\frac{1}{\nu^2}\right)(\nu)^{l+1} \\ W_{\nu,l+1/2}\left(\frac{2r}{\nu}\right) &= \frac{\Gamma(l+1+\nu)}{(-\nu)^{l+1}}\left[G_l\left(2r,\frac{1}{\nu^2}\right)\cos\pi\nu + H_l\left(2r,\frac{1}{\nu^2}\right)\sin\nu\right], \end{aligned} \tag{15}$$

where G_l and H_l are slowly varying functions of $1/\nu^2$. Then

$$\begin{aligned} \frac{f_{N,2}}{f_{N,1}} &= -\frac{(f_{N-1,1}[M_\nu, M_{\alpha_{N-1}}]+f_{i-1,2}[M_\nu, W_{\alpha_{N-1}}])}{(f_{N-1,1}[W_\nu, M_{\alpha_{N-1}}]+f_{N-1,2}[W_\nu, W_{\alpha_{N-1}}])} \\ &= \frac{[(-1)^l\Gamma(2l+2)/\Gamma(l+1+\nu)](f_{i,1}[G_l, M_{\alpha_{N-1}}]+f_{i,2}[G_l, W_{\alpha_{N-1}}])}{\cos\pi\nu(f_{N-1,1}[G_l, M_{\alpha_{N-1}}]+f_{N-1,2}[G_l, W_{\alpha_{N-1}}])+\sin\pi\nu(f_{N-1,1}[H_l, M_{\alpha_{N-1}}]+f_{N-1,2}[H_l, W_{\alpha_{N-1}}])}. \end{aligned} \tag{16}$$

Let

$$\begin{aligned} D &= \{(f_{N-1,1}[G_l, M_{\alpha_{N-1}}]+f_{N-2,2}[G_l, W_{\alpha_{N-1}}])^2+(f_{N-1,1}[H_l, M_{\alpha_{N-1}}]+f_{N-1,2}[H_l, W_{\alpha_{N-1}}])^2\}^{1/2}, \\ \sin\pi(\mu_l+l) &= (f_{N-1,1}[G_l, M_{\alpha_{N-1}}]+f_{N-1,2}[G_l, W_{\alpha_{N-1}}])/D, \\ \cos\pi(\mu_l+l) &= (f_{N-1,1}[H_l, M_{\alpha_{N-1}}]+f_{N-1,2}[H_l, W_{\alpha_{N-1}}])/D, \end{aligned} \tag{17}$$

where μ_l is defined as the quantum defect. Then,

$$\frac{f_{N,2}}{f_{N,1}} = \frac{\Gamma(2l+2)\sin\pi(\mu_l+l)}{\Gamma(l+1+\nu)\sin\pi(\mu_l+\nu)} \tag{18}$$

and

$$g(r,r',E) = -\frac{1}{(r_<)(r_>)}\,\frac{\nu}{2}\left[\frac{\Gamma(l+1-\nu)}{\Gamma(2l+2)}\,M_{\nu,l+1/2}\left(\frac{2r_<}{\nu}\right)+\frac{\Gamma(l+1-\nu)}{\Gamma(l+1+\nu)}\,\frac{\sin\pi(\mu_l+l)}{\sin\pi(\mu_l+\nu)}\,W_{\nu,l+1/2}\left(\frac{2r_<}{\nu}\right)\right]W_{\nu,l+1/2}\left(\frac{2r_<}{\nu}\right). \tag{19}$$

Equation (18) differs from the widely quoted expressions of Ref. 8 by a factor $\pm\frac{1}{2}$. The factor $\frac{1}{2}$ arises from the use of rydbergs rather than hartrees, and the sign has been discussed above. To illustrate the agreement of the model potential and the Herman-Skillman potential,[16] Table I lists the Z_i and r_i parameters of the model potential for Cs, the one-electron eigenvalues (in Ry), and a comparison of experimental[22] and model effective principal quantum numbers. The model eigenvalues agree with those of Herman and Skillman[16] to better than 3%. The 6*s* effective principal quantum number (n^*) is 1.970 with the model, 1.954 with the Herman-Skillman potential, but experimentally, it is 1.869. In Mann's[23] Hartree-Fock calculations the n^* for the 6*s* electron, obtained from the orbital binding energy is 2.011. Thus, while the model potential does not reproduce the measured 6*s* ionization energy, it is no worse in this respect than other, more sophisticated approaches. In comparison with experiment the *ns* and *np* levels are too loosely bound. Small parameter variations in the potential do not significantly affect the n^* values. Large parameter variations can improve the agreement with experimental *ns* and *np* levels but the price is to greatly enhance the difference with *nd* levels. It is concluded that the difference between model and experimental n^* values is inherent in the use of a one-electron model.

The generalized cross sections used here are obtained from the transition rate

$$\frac{dW}{dt}\,(\mathrm{sec}^{-1}) = \sum_{n=1}^{\infty}\sigma_n F^n,$$

where F is the photon flux in number/cm^2 sec, and σ_n is in units cm^{2n} sec^{n-1}. For two-photon absorption from an initial *s* orbital

$$\begin{aligned} \sigma_2^L &= 4\pi(\Delta E/F_0)^2\tfrac{1}{9}[(R^2_{010})^2+\tfrac{4}{5}(R^2_{012})^2], \\ \sigma_2^C &= 4\pi(\Delta E/F_0)^2\,\tfrac{2}{15}(R^2_{012})^2, \end{aligned} \tag{20}$$

TABLE I. Model parameters Z and r for Cs. For bound levels the model and Herman-Skillman (HS) eigenvalues (Ry) are listed. For excited levels the model and experimental (Ref. 22) effective principal quantum numbers are listed.

N	1	2	3	4	5	6	7	8	9
Z	55.0	47.0	39.1	28.0	19.4	9.80	5.40	2.00	1.00
R	0.070	0.155	0.335	0.570	1.02	1.78	2.95	4.10	

level	E(mod)	E(HS)	level	n^*(mod)	n^*(expt)
$1s$	2572	2531	$6s$	1.9700	1.8688
$2s$	381.6	389.5	$7s$	2.9898	2.919
$2p$	357.8	368.0	$8s$	3.9963	3.933
$3s$	81.12	81.91	$9s$	4.9994	4.939
$3p$	71.91	72.60	$6p$	2.3925	2.350
$3d$	53.84	55.14	$7p$	3.4217	3.394
$4s$	15.85	15.79	$8p$	4.4322	4.409
$4p$	12.45	12.39	$9p$	5.4373	5.415
$4d$	6.332	6.437	$10p$	6.4401	6.419
$5s$	2.133	2.119	$5d$	2.5655	2.551
$5p$	1.254	1.254	$6d$	3.4772	3.532
$6s$	0.258	0.262	$7d$	4.4622	4.529
			$8d$	5.4572	5.528

where ΔE is the photon energy in rydbergs, the superscripts L and C refer to linear and circularly polarized radiation, $F_0 = 3.22\times10^{34}/\mathrm{cm}^2\,\mathrm{sec}$ and

$$R^2_{l_1 l_2 l_f} = \int_0^\infty r_1^3 dr_1 \Psi_{l_1}(r_1) \times \int_0^\infty r_2^3 dr_2 \Psi_{l_f}(r_2) g_{l_2}(r_1, r_2, E_i - \omega)$$

and we use the rydberg Green's function. For three-photon absorption from an s orbital

$$\sigma_3^L = 8\pi(\Delta E/F_0)^3[\tfrac{1}{27}(R^3_{0101} + \tfrac{4}{5}R^3_{0121})^2 + \tfrac{4}{175}(R^3_{0123})^2],$$
$$\sigma_3^C = 8\pi(\Delta E/F_0)^3 \tfrac{2}{35}(R^3_{0123})^2, \qquad (21)$$

where

$$R^3_{l_1 l_2 l_3 l_f} = \int_0^\infty r_1^3 dr_1 \Psi_{l_1}(r_1) \int_0^\infty r_2^3 dr_2 g_{l_2}(r_1, r_2, E_i - \omega) \int_0^\infty r_3^3 dr_3 \Psi_{l_f}(r_3) g_{l_3}(r_2, r_3, E_i - 2\omega).$$

These expressions differ from ones given by Manakov[24] *et al.* by a factor 2^{N-1}. The difference arises from using hartree rather than rydberg energy units, and is accounted for by the product of factors 2^{-N} from the $(\Delta E/F_0)$ coefficient, 2^{2N-2} from the Green's function, and 2^1 from the normalization of the continuum orbitals. Alternative expressions exist in the literature,[6,14] with the difference arising from the continuum electron normalization.

The ratio of cross sections for circular to linear polarized light ($R_N = \sigma_N^C/\sigma_N^L$) is a useful quantity. For two-photon absorption $R_2 = 1.5$ when $R^2_{012} \gg R^2_{010}$, and $R_2 = 0$ when $R^2_{010} \gg R^2_{012}$. For three-photon absorption $R = 2.5$ when R^3_{0123} dominates $(R^3_{0101} + 0.8R^3_{0121})$, i.e., when either R^3_{0123} is large or when $R^3_{0101} = -0.8R^3_{0121}$.

III. THREE-PHOTON IONIZATION OF THE He$(1s)(2s)^1$ ^3S METASTABLE LEVEL

Three-photon ionization of the He metastable levels is of interest as there exist a variety of discordant calculations[25] and some measurements. Bakos *et al.*[26] measure a cross section of $10^{-78+1.6}_{-1.3}$ cm^6 sec^2 for three-photon ionization of the ^1S metastable at 6944 Å (ruby laser wavelength). The error bars in the measurement are so large that it is irrelevant to the intercomparison of various computations. In Figs. 1(a) and 1(b) my calculated three-photon ionization cross section for the ^1S and ^3S metastable levels in He are shown. Also shown are the ratios (R) of circular cross section to linear cross section.

These figures illustrate some general points. The predicted resonance position (solid lines) differ from the expected experimental positions (dashed lines). In He this is due to the neglect of electrostatic splitting in the $(1s)(nl)$ intermediate configurations. The maximum value of R is 2.5 from Eq. (71). This is approached but generally not reached at nd resonances, because

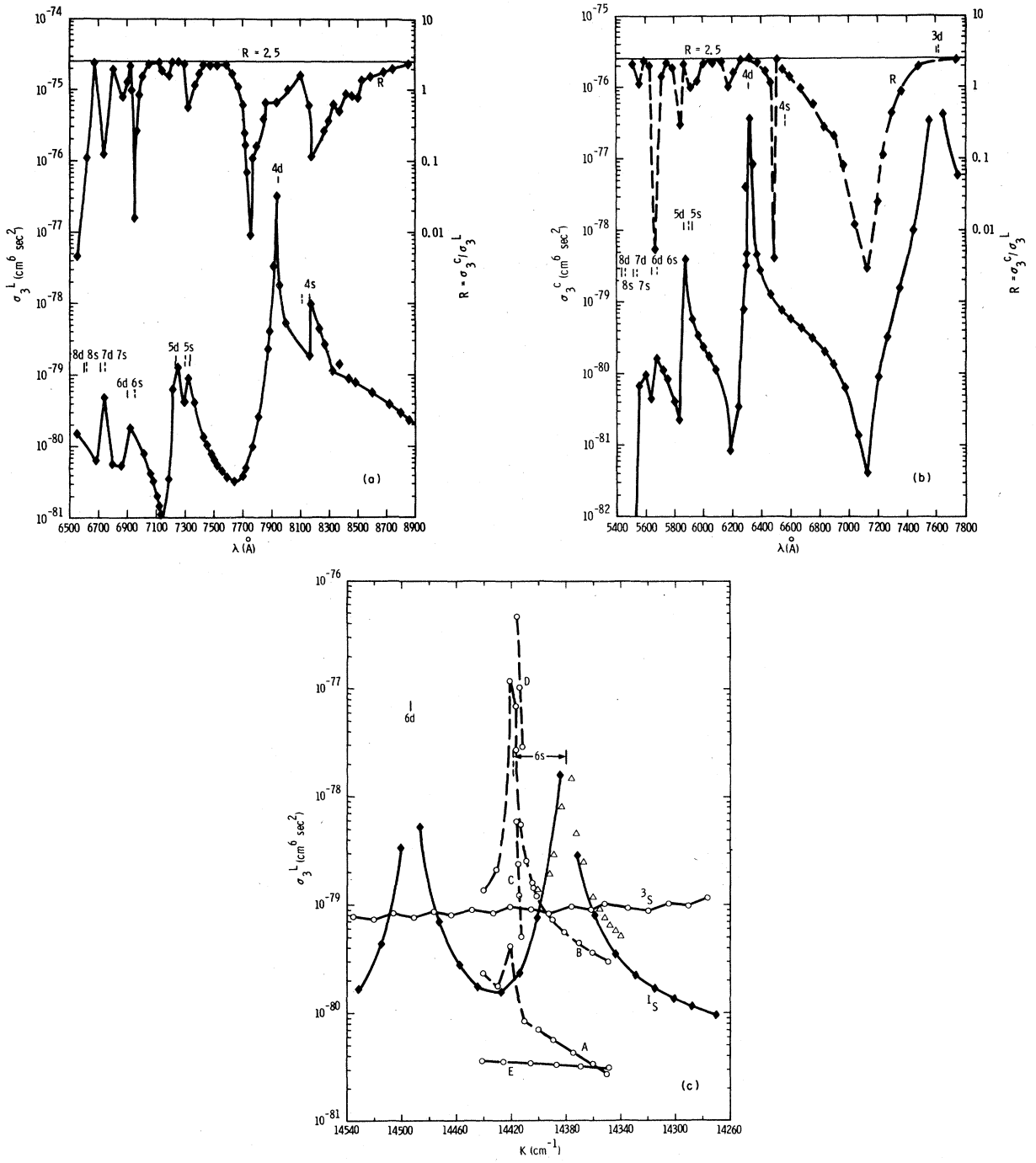

FIG. 1. (a) σ_3^L and R vs λ for He $(1s)(2s)\,^1S$. (b) σ_3^C and R vs λ for He $(1s)(2s)\,^3S$. (c) σ_3^L for He $(1s)(2s)\,^1S$ and ^3S (solid curves). The dashed curves A–E are from Ref. 25 and discussed in the text. The open triangles are curve B shifted downward by 40 cm^{-1}.

both R_{0121} and R_{0123} diverge, but R_{0121} is not present in σ_3^C. At (ns) resonances $R=0$, but this is not apparent in the figures as the resonances are narrow and the calculations are done at only 60 points.

Figure 1(c) is a detail of the cross sections near 6944 Å (14 400 cm^{-1}). In this region (14 540–14 260 cm^{-1}) for linearly polarized light the triplet cross section is flat while the singlet cross section (solid curve) contains both the 6s and 6d reso-

nances. The calculated position of the 6s resonance (14 380 cm^{-1}) differs from its expected experimental position (14 420 cm^{-1}) by 40 cm^{-1} [the measured He (1s)(6s) ^1S-^3S splitting in 80 cm^{-1} and electrostatic splitting has been neglected]. Also shown are four other calculations (A–D) near the resonance at 14 420 cm^{-1}. Curve A is the truncated sum calculation of Olsen *et al.*[25] It is an order of magnitude lower than the other calculations at lower wave numbers. Curve B is the QDM calculations of Olsen *et al.*[25] Except for the 40 cm^{-1} difference in resonance position curve B is in excellent agreement with my results. The triangles in Fig. 1(c) are points on curve B shifted 40 cm^{-1}, showing the excellent agreement in shape and magnitude of the two calculations. Curves C and D are alternative calculations reported by Bakos *et al.*,[26] and in comparison with curve B show the variability in reported QDM calculations. Curve E is the QDM ^3S cross section of Olsen *et al.*[25] It is at least an order of magnitude below my cross section (the solid curve).

Bakos *et al.*[26] report a ratio $\sigma_3^L(^1S)/\sigma_3^L(^3S) = 10 \pm 5.3$ at 14 412 cm^{-1}. At 14 372 cm^{-1} I calculate a ratio of three. However, Bakos *et al.* measure $1/R(^1S) = 0.5 \pm 0.15$ at 14 414 cm^{-1} and $1/R(^3S) = 0.35 \pm 0.15$ at 14 407 cm^{-1}. At 14 371 cm^{-1} I calculate $1/R(^1S) = 12.2$, and $1/R(^3S) = 10.8$ at 14 406 cm^{-1}. The QDM calculation of Olsen *et al.* is $1/R(^1S) = 6.36$ at 14 414 cm^{-1} and $1/R(^3S) = 1.93$ at 14 407 cm^{-1}. The values of $1/R$ measured by Bakos *et al.* indicate both ^1S and ^3S cross sections are dominated by R^3_{0123}, i.e., they are close to the limit $1/R = 0.40$. But there is no nd resonance at 14 414 cm^{-1}. Further, my ^3S calculations indicate a large dip in $R(^3S)$ between 6600 and 7400 Å (13 500–15 150 cm^{-1}), which arises from a zero in R^3_{0123} in the ^3S calculation, while the small value of $R(^1S)$ is due to the 6s resonance.

Lompré *et al.*[27] have recently measured $\sigma_3^L(^1S)$ and $\sigma_3^L(^3S)$ at 14 398.5 cm^{-1}. They find $\sigma_3^L(^1S) = 3.3 \pm 1.9 \times 10^{-80}$, somewhat smaller than the calculation of Olsen *et al.*[25] (1.6×10^{-19}) at 14 400 cm^{-1}, and my value 8×10^{-80} at 14 360 cm^{-1} (with a 40 cm^{-1} shift). There is a significant disagreement between theory and experiment for the ratio $\sigma_3^L(^1S)/\sigma_3^L(^3S)$ at this wavelength. Lompré *et al.*[27] measure a ratio of 11, in agreement with the ratio measured by Bakos *et al.*, Olsen *et al.*[25] (at 14 400 cm^{-1}) calculate a ratio of 34, while I find a ratio of 1. The value of $\sigma_3^L(^3S)$ obtained from the measurement of Lompré *et al.*[27] is in excellent agreement with the calculation of Olsen *et al.* The large disagreement in $\sigma_3^L(^3S)$ far from any resonances suggest that a measurements on σ_3^L for Li would be useful.

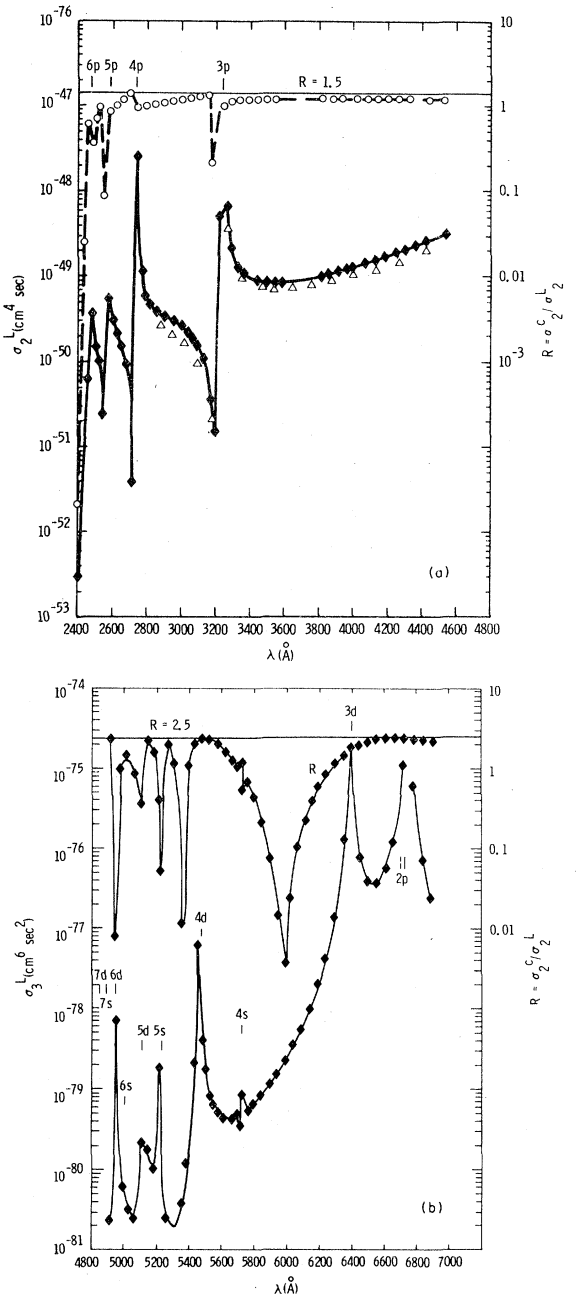

FIG. 2. (a) σ_2^L and R vs λ for Li. The open triangles are the calculations of Ref. 28. (b) σ_3^L and R vs λ for Li.

IV. TWO- AND THREE-PHOTON IONIZATION OF LITHIUM

Except for the 2p, the calculated n^* values for excited states in Li were in good agreement with the experimental values [to the resolution of the wavelength scale used in Figs. 2(a) and 2(b)]. The results for two-photon ionization are shown in

Fig. 2(a). As mentioned in Sec. II, $R=1.5$ corresponds to $R^2_{012} \gg R^2_{010}$. Near the np resonances both R^2_{010} and R^2_{012} go through zero (antiresonances) but in the calculations they do not go through antiresonance at the same wavelength. This accounts for the structure in R near the resonances. Between 3400 and 4500 Å, $R=1.24\pm0.04$. At 3472 Å Manakov *et al.*[24] find $R=1.42$, and $\sigma^C_2=3.44\times10^{-49}$, whereas I find $\sigma^C_2=0.70\times10^{-49}$ cm^4 sec. The triangles in Fig. 2(a) are Mizuno's[28] calculations for σ^L_2. My results are in good agreement with Mizuno's.

The results for three-photon ionization in Li are shown in Fig. 2(b). The broad dip in R at 5960 Å is the result of a zero in R^3_{0123} as was seen in $R(^3S)$ in He at 7100 Å. A small dip in R and peak in σ^L_3 is seen at 5724 Å due to the $4s$ resonance, a surprisingly narrow structure. At 5300 Å Manakov *et al.*[24] find $\sigma^L_3=7.1\times10^{-82}$ and $R=0.045$, whereas I find $\sigma^L_3=2.0\times10^{-81}$ and $R=1.16$. Near 5300 Å there is a zero in my calculated R_{0101}, and this probably accounts for the difference in the two calculated R values.

V. TWO- AND THREE-PHOTON IONIZATION IN Na

In Fig. 3(a) the two photon cross section and R values are shown. At 3472 Å Manakov *et al.*[24] find $\sigma^C_2=5.6\times10^{-52}$ cm^4 sec and $R=0.89$, while I find $\sigma^C_2=2.4\times10^{-51}$ and $R=0.75$. With the resolution used, no variation was found in R at 3300 Å the $4p$ resonance. The structure in R and σ^C_2 near 3600 Å arises from a zero in R^2_{012}. The open triangles in Fig. 3(a) are Mizuno's[28] calculations for σ^C_2. My calculations are in excellent agreement with those of Mizuno except for a 120 Å difference in the location of the minimum due to a zero in R^2_{012}.

In Fig. 3(b) the three-photon cross section σ^C_3 and $R=\sigma^C_3/\sigma^L_3$ are shown. At shorter wavelengths both quantities show considerable structure. The departure of the model n^* values from experiment and the resulting difference in resonance position are shown by the solid and dashed markers. At 5300 Å I calculate $\sigma^L_3=1.1\times10^{-80}$ and $R=0.80$. Manakov *et al.*[24] find $\sigma^L_3=7.8\times10^{-79}$ cm^6 sec^2 and $R=0.33$, while Delone *et al.*[29] measure $R=0.42\pm20\%$. The large R value I find arises from a zero in R^3_{0101} near 5300 Å. At 6944 Å I calculate $\sigma^L_3=7\times10^{-78}$ cm^6 sec^2 and $R=2.49$. Manakov *et al.*[24] calculate $\sigma^L_3=9.3\times10^{-78}$ cm^6 sec^2 and $R=2.49$, while Isenor[30] reports $\sigma^L_3=56.0\times10^{-78}$ cm^6 sec^2 and $R=2.35\pm0.10$. Figure 3(b) indicates that R is not a sensitive function of λ near 6944 Å. At this wavelength the two calculations are in agreement but the absolute cross section is a factor of six lower than experiment. The plateau regions in R near the $3d$ and $4d$ resonances result from the dominance of the matrix element R^3_{0123}. The dip in R between 6000 and 6400 Å results from a zero in R^3_{0101} near the $5s$ resonance. This structure is substantially broader than the comparable structure, near the $4s$ resonance, in Li. Clearly, measurements of R for three-photon ionization over a broad spectral region would be interesting. Fea-

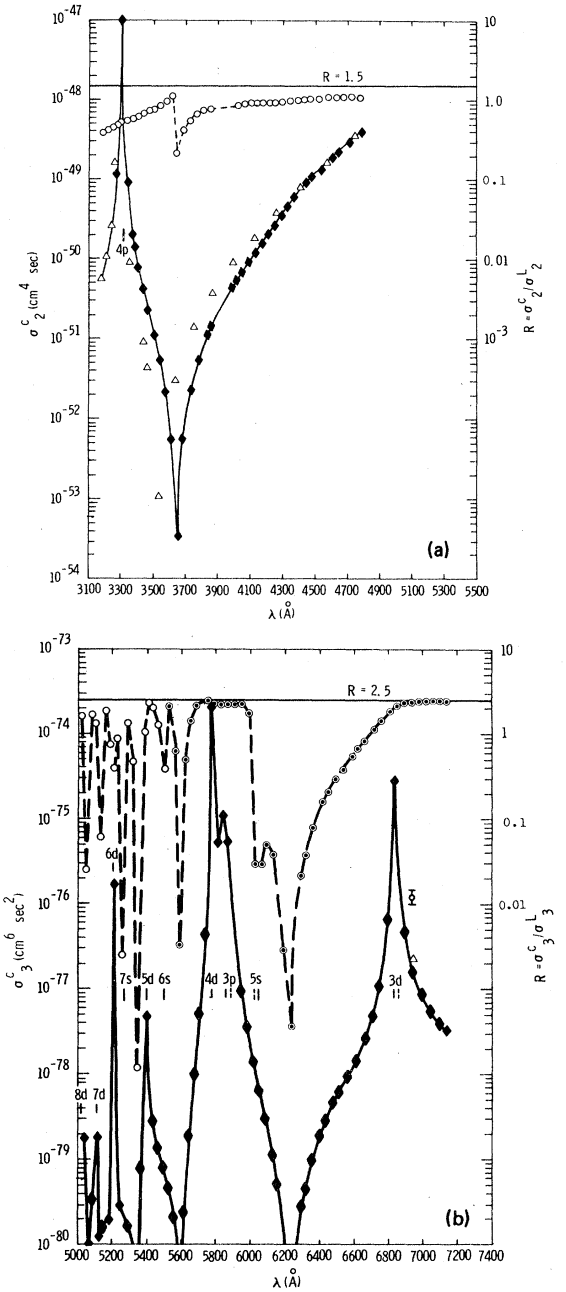

FIG. 3. σ^C_2 and R vs λ for Na. The open triangles are the calculations of Ref. 28. (b) σ^C_3 and R vs λ for Na. The data point with error bars and open triangle at 6944 Å are from Refs. 30 and 24, respectively.

tures arising from zeros in matrix elements are of special interest as they are a test of the calculational procedures.

VI. TWO- AND THREE-PHOTON IONIZATION IN K

Of the elements studied with the one-electron model, the excited levels of potassium showed the greatest departure from experiment. Table II compares the model and experimental[22] n^* values. The ns and np levels are less tightly bound than the experimental levels, but nd n^* values are significantly smaller than those measured. At $Z=21$ the $3d$ shell is partially occupied in the ground state, and in going from $Z=18$ to $Z=21$, the nd orbitals show a rapid decrease in n^*. In my one-electron model, the decrease is too rapid. However, the disparity in n^* values provides a testing ground for adjusting the wavelength scale so that resonances occur at their experimental energy.

In Fig. 4(a) the two-photon cross section and R values are shown. The difference between model and experimental resonance positions is small, and is shown by solid and dashed markers. The dips in R arise from zeros in R^2_{012}. At 3742 Å, Manakov *et al.*[24] calculate $\sigma_2^C = 3.3\times10^{-50}$ and $R=1.08$, while I find $\sigma_2^C = 3.5\times10^{-50}$ cm^4 sec, and $R=1.0$; excellent agreement. At 5300 Å Manakov *et al.* calculate $\sigma_2^C = 1.9\times10^{-49}$ and $R=1.16$, while I find $\sigma_2^C = 5.4\times10^{-49}$ cm^4 sec and $R=1.28$. Delone *et al.*[28] measure $R=1.2\pm30\%$ at 5300 Å. The two calculated R values are within experimental error, and the cross sections agree to a factor of three. The open triangles in Fig. 4(a) are calculations of Mizuno.[28] Unlike Li and Na where there is good agreement, for K my calculations and Mizuno's differ by as much as a factor of three.

In Fig. 4(b) the three-photon ionization cross section σ_3^C and R values are shown. The figure illustrates several interesting points. Isenor[30] reports $\sigma_3^C = 0.93\times10^{-78}$ cm^6 sec^2 at 6944 Å where Manakov *et al.*[24] calculate $\sigma_3^C = 0.46\times10^{-78}$ cm^1 sec^2. In Fig. 4(b) the measurement is in the wings of the $5d$ resonance, and my calculated $5d$ resonance is 160 Å higher in wavelength than its experimental position. Shifting the Isenor measurement 160 Å upward in wavelength leads to excellent agreement with my calculation. However, Isenor reports $R=2.66\pm0.11$, Manakov *et al.* calculate $R=2.49$, while I find $R=1.3$ at 7100 Å. The broad dip in my calculated R is due to a zero in R^3_{0123} at 7260 Å.

With this 160 Å shift in wavelength scale, the calculation is in good (factor of two) agreement with the measurement. However, between 7300 and 7700 Å there are resonances due to $4d$ and $4p$ levels, and the resonances are interchanged in the model calculation. No simple shift in wavelength scale can predict a cross section with experimental resonance energies. However, as the $4p$ resonance occurs in the $4s$-νp matrix element and the $4d$ resonance in the νd-ϵl matrix element one can separately modify the E_i value to reproduce both resonances at their experimental energies. The results of the calculation are shown in Fig. 4(c), where the modified cross section and R are shown as solid lines and the results from Fig. 4(b) as dashed lines and solid triangles. Alternatively, one may use the finite sum subtraction technique, mentioned in the introduction. Here the terms $|4p\rangle\langle 4p|[1/(\lambda - E_{4p}) - 1/(\lambda - E^0_{4p})]$ and $|4d\rangle\langle 4d|[1/(\lambda - E_{4d}) - 1/(\lambda - E^0_{4d})]$, were included in the modified Green's function. The results for σ_3^C and R are shown as open and solid circles, respectively. The σ_3^C values calculated with modified Green's function and unmodified energies is in good agreement near the resonances with σ_3^C calculated with unmodified Green's function and modified energies. The R values differ principally due to the distortion introduced by the energy modification, i.e., the location of the $6s$ resonance and the zero in R_{0123} are shifted to shorter wavelength by 330 Å, the shift in the $4d$ resonance. Teague and Lambropoulos[31,32] have calculated σ_3^C near the $4p$ resonance. Their results are shown as open squares in Fig. 4(c). Their resonance is considerably narrower than in my calculation.

TABLE II. Model and experimental (Ref. 22) effective principal quantum numbers for K and Rb.

K					
	n^*			n^*	
Level	model	expt	level	model	expt
$4s$	1.821	1.770	$6p$	4.301	4.273
$5s$	2.834	2.801	$7p$	5.304	
$6s$	3.838	3.809	$3d$	2.740	2.853
$7s$	4.840	4.812	$4d$	3.532	3.795
$8s$	5.841	5.814	$5d$	4.452	4.768
$4p$	2.270	2.233	$6d$	5.419	
$5p$	3.293	3.264			

Rb					
	n^*			n^*	
Level	model	expt	level	model	expt
$5s$	1.870	1.804	$7p$	4.368	4.337
$6s$	2.886	2.844	$8p$	5.373	
$7s$	3.891	3.855	$4d$	2.729	2.766
$8s$	4.893	4.860	$5d$	3.595	3.705
$9s$	5.894	5.862	$6d$	4.548	4.683
$5p$	2.334	2.292	$7d$	5.529	
$6p$	3.359	3.325	$8d$	6.519	

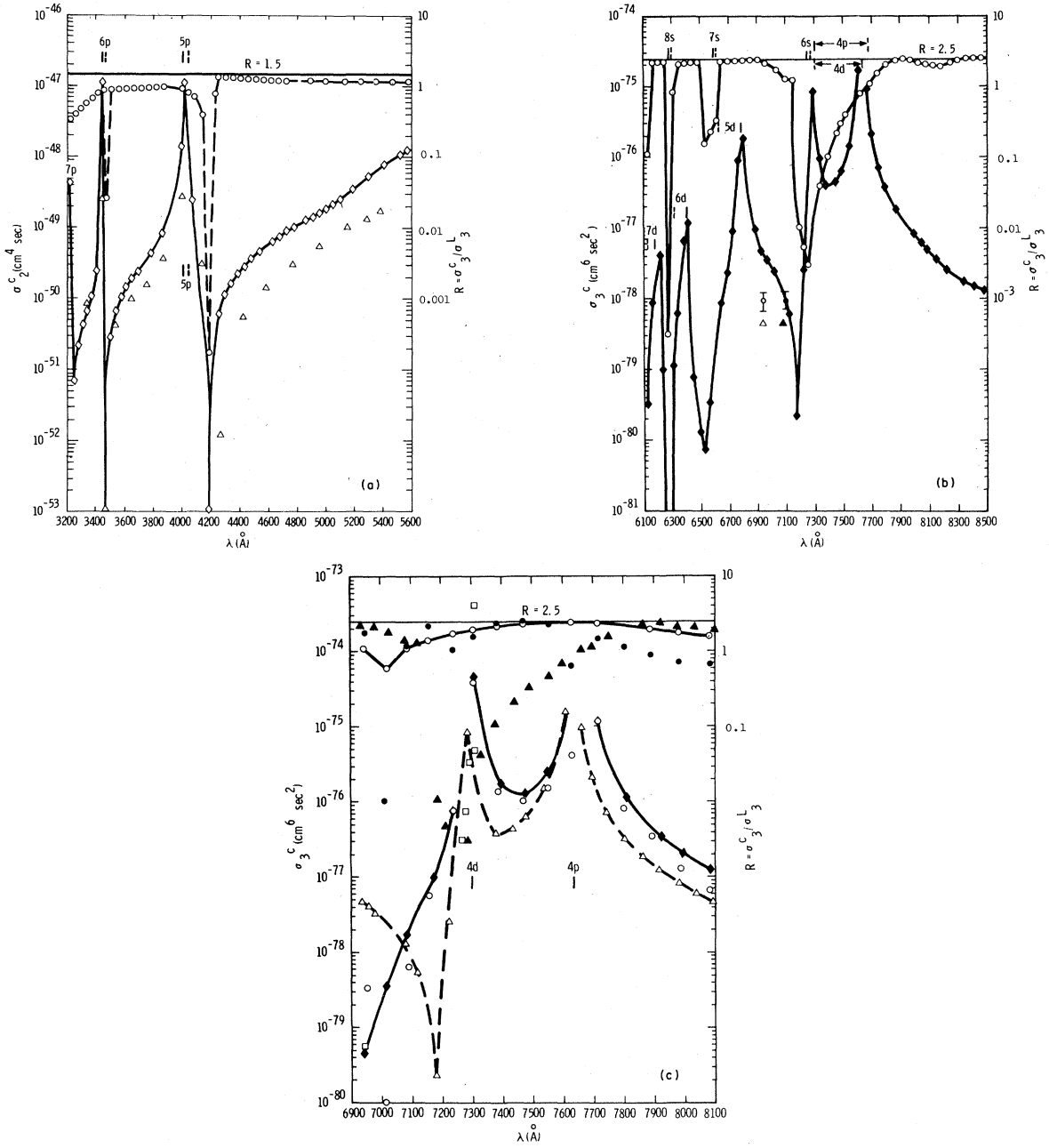

FIG. 4. (a) σ_2^C and R vs λ for K. The open triangles are the calculations of Ref. 28. (b) σ_3^C and R vs λ for K. The data points with error bars and triangles are from Refs. 30 and 24, respectively. They are shown at 6944 and 7100 Å, the latter to account for the shift of the $5d$ resonance in the model. (c) The solid curves are σ_3^C and R, adjusted so the $4d$ and $4p$ resonances occur at their experimental energy. The dashed curve and solid triangles are the unadjusted model values from Fig. 4(b). The open and closed circles are σ_3^C and R, respectively, obtained with a modified Green's function.

VII. TWO- AND THREE-PHOTON IONIZATION IN Rb

The model and experimental n^* values for Rb are listed in Table II. As with K the model ns and np n^* values are larger than the experimental values. The model n^* values for nd are smaller than the experimental values, but the difference is not as large as in K, i.e., the experimental n^* values are lower and model n^* values higher in Rb than in K.

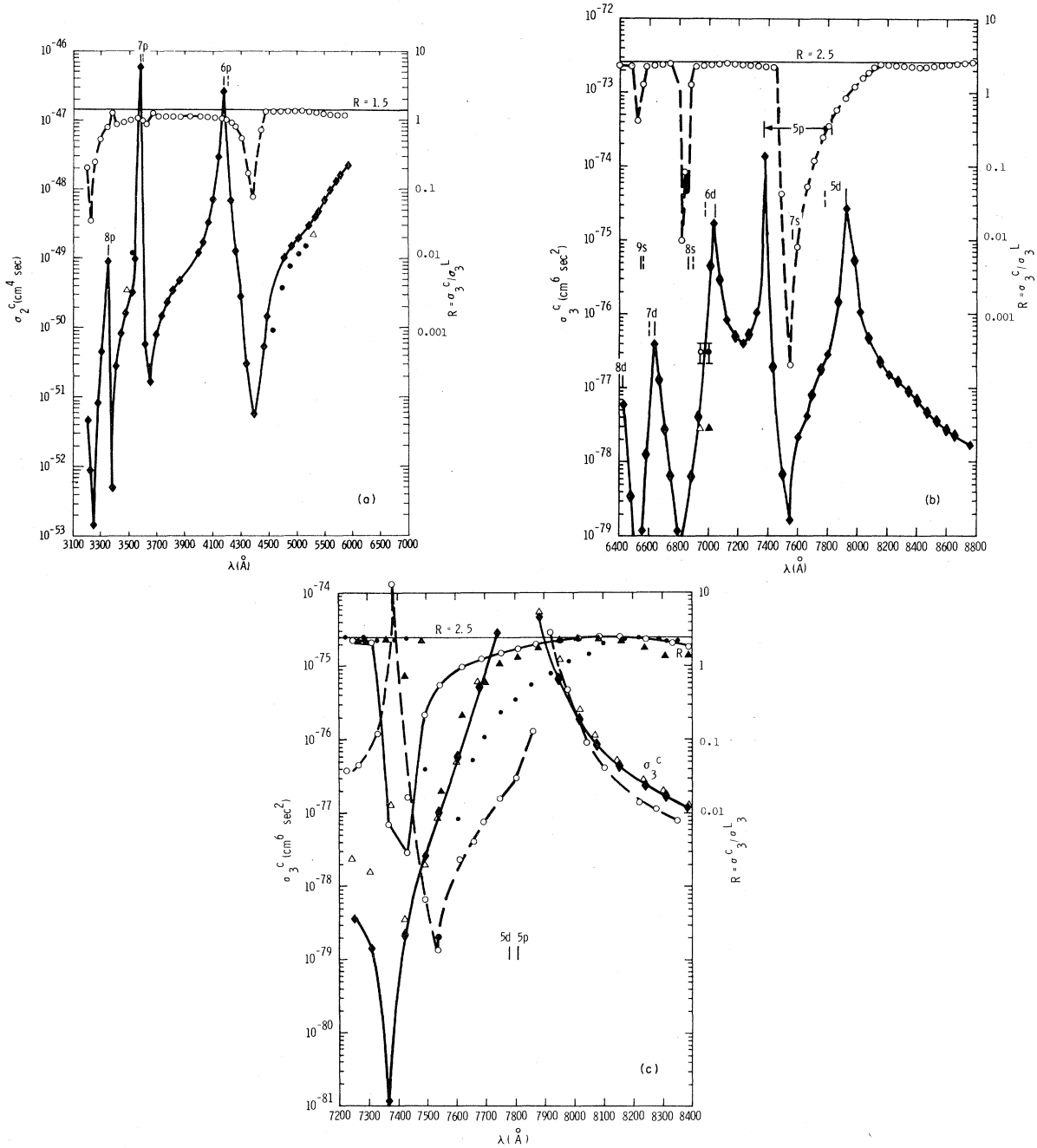

FIG. 5. (a) σ_2^C and R vs λ for Rb. The open triangles and solid circles are the calculations of Refs. 24 and 33, respectively. (b) σ_3^C and R vs λ for Rb. The data points with error bars and triangles are from Refs. 30 and 24, respectively. They are shown at 6944 and 7000 Å, the latter to account for the shift of the $6d$ resonance in the model. (c) The solid curves are σ_3^C and R, adjusted so the $5d$ and $5p$ resonances occur at their experimental energy. The dashed curve and solid circles are the unadjusted model values from Fig. 5(b). The open and solid triangles are σ_3^C and R, respectively, obtained with a modified Green's function.

In Fig. 5(a) the two-photon cross section σ_2^C and R are shown. Also shown are calculated values of Manakov *et al.*[24] (open triangles) and Lambropoulos and Teague,[33] (solid circles) both using the QDM method. The three calculated cross sections agree to a factor of two. At 3472 and 5300 Å Manakov *et al.* calculate $R = 1.43$ and 2.14, respectively, while I calculate $R = 1.00$ and 1.39, at

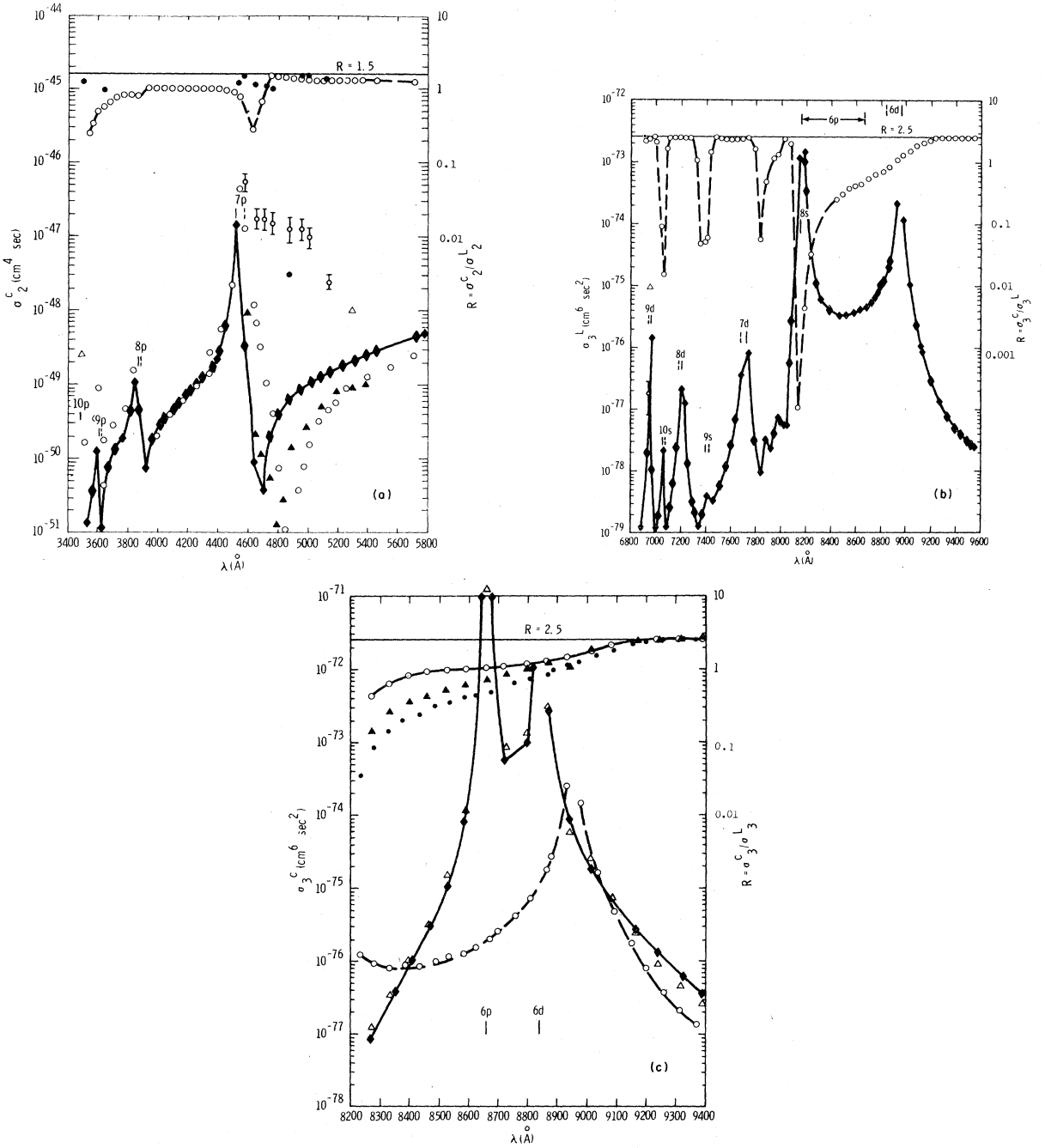

FIG. 6. (a) σ_2^C and R vs λ for Cs. The open and solid circles are σ_2^C and R calculated in Ref. 32. The data points with error bars are from Ref. 34. The solid triangles are recent data from Ref. 40. (b) σ_3^L and R vs λ for Cs. The data point with error bars and open triangle at 6944 Å are from Refs. 30 and 24, respectively. (c) The solid curves are σ_3^C and R, adjusted so the 6*d* and 6*p* resonances occur at their experimental energy. The dashed curves and solid circles are the unadjusted model values from Fig. 6(b). The open and solid triangles are σ_3^C and R, respectively, obtained with a modified Green's function.

the same wavelengths.

In Fig. 5(b) the three-photon cross section σ_3^C and R values are shown. As with K, in Rb the 5*p* and 5*d* resonance positions are interchanged. R goes to zero at the *ns* resonance, and in addition, near 6825 and 7520 Å where R_{0123}^3 has zeros. The 6*d* resonance in the model is 60 Å above its expected experimental position. Measurements at

6944 Å are in the tail of the $6d$ resonance. The measured σ_3^C reported by Isenor[30] and the calculated value of Manakov *et al.*[24] are shown both at 6944 and 7004 Å. My calculated cross section is in reasonable agreement with the shifted measured value. At 7004 Å my calculated $R = 2.44$. At 6944 Å Isenor[30] reports a measured value of $R = 2.16 \pm 0.13$, Delone *et al.*[29] measure $R = 2.17 \pm .13$, and Manakov *et al.*[24] calculate 2.35.

In Fig. 5(c) are shown σ_3^C and R (solid lines) calculated with E_i modified to produce $5p$ and $5d$ resonances at their experimental positions. σ_3^C and R without the energy modification are shown as a dashed curve and solid circles, respectively. Also shown are σ_3^C and R (open and solid triangles) calculated using model energies but a modified Green's function, i.e., $|5p\rangle\langle 5p|[1/(\lambda - E_{5p}) - 1/(\lambda - E_{5p}^0)]$ and $|5d\rangle\langle 5d|[1/(\lambda - E_{5d}) - 1(\lambda - E_{5d}^0)]$. Near the resonances σ_3^C calculated with different modifications are in excellent agreement. Near 7300 Å there is a dip in R and a peak in σ_3^C in the calculation with modified Green's function. This is a numerical artifact resulting from the subtraction of two large numbers. At 7380 Å the unmodified calculation leads to σ_3^L three orders of magnitude larger than in the modified Green's function calculation. Near 7500 Å there is a zero in R_{0123} and in R, and its position varies in the three calculations.

VIII. TWO- AND THREE-PHOTON IONIZATION OF Cs

Over the past five years the two-photon ionization cross section of Cs has received substantial experimental[34,35] and theoretical[36-38] attention; the reason being the orders of magnitude disagreement between theory and experiment for $4600 \leq \lambda \leq 5200$ Å. However, the recent remeasurements of the two-photon cross section by Normand and Morellec,[39] and by Morellec *et al.*[40] have resolved the disagreement. In Fig. 6(a) I show my calculated cross section σ_2^C as a solid line and R as a series of connected open circles. The calculated σ_2^C values of Lambropoulos and Teaque[33] are shown as isolated open circles and their R values as solid circles. The calculated σ_2^C values of Manakov *et al.*[24] are shown as open triangles. With allowance for the 50 Å shift in $7p$ resonance position my calculations are in reasonable agreement with those of Lambropoulos and Teaque, though the agreement is only qualitative near 4800 Å (the dip in σ_3^L). The measurements of Granneman and Van der Wiel[34] are shown as open circles with error bars. The measurements of Morellec *et al.*[40] are shown as solid triangles (they measured σ_3^L which I converted to σ_3^C with my calculated R values). The calculation of Lambropoulos and Teaque[33] is in good agreement with the measurement of Morellec *et al.*,[40] considering the difficulty in accurately locating the cross-section minimum. My calculations are somewhat higher than the measurements. This arises from the incorrect location of the $6p$ level with the Green's-function approach, and could be corrected by including a term of the form $|6p\rangle\langle 6p|[(1/(\lambda - E_{6p}) - (1/\lambda - E_{6p}^0)]$.

The calculated three-photon cross section σ_3^L and R values are shown in Fig. 6(b). The calculation is in excellent agreement with the measurement reported by Isenor[30] at 6944 Å, when the $9d$ resonance peak is shifted 20 Å, to bring it into agreement with the expected experimental $9d$ resonance energy. At 6944 Å the calculation of Manakov *et al.*[24] is an order of magnitude larger. At 6944 Å Isenor[30] reports $R = 2.24 \pm 0.11$, I calculate $R = 2.25$, while Mankov *et al.*[24] find $R = 1.45$.

In Fig. 6(c) the three-photon cross section σ_3^C is plotted for $8200 \leq \lambda \leq 9400$ Å. The solid curves for σ_3^C and R were obtained with an energy adjustment to produce the $6p$ and $6d$ resonances at their true energy. The dashed curve and solid circles are σ_3^C and R without the energy modification. The solid and open triangles are σ_3^C and R without the energy modification but including $(|6p\rangle\langle 6p|[1/(\lambda - E_{6p}) - 1/(\lambda - E_{6p}^0)]$ and $(|6d\rangle\langle 6d|[1/(\lambda - E_{6d}) - 1/(\lambda - E_{6D}^0)]$ as discussed in the introduction. This modification produces a σ_3^C in excellent agreement with that obtained with the energy modification. The R value is significantly different at shorter wavelengths because the energy modification distorts the location of the $8s$ resonance, affecting σ_3^L but not σ_3^C.

IX. CONCLUSIONS

It has been shown that the infinite sums appearing in multiphoton absorption matrix elements can be replaced by atomic Green's functions, and I have shown that an explicit Green's function can be constructed for realistic one-electron atomic central potentials. The multiphoton absorption matrix element is then reduced to angular-momentum coupling coefficients and multiple integrals, which are approximated as sequential sums. For one-electron systems, the multiphoton absorption matrix element is then no more difficult to calculate than a one-photon absorption matrix element. The disadvantage in the model Green's-function approach is that the resonances occur at model eigenvalues, not at experimental energy levels. In two-photon absorption this is not a serious problem as the model eigenvalues and experimental energy levels are in reasonable agree-

ment. The wavelength scale can be shifted slightly to move the calculated resonances to the experimental energies. In three-photon ionization the differences between model eigenvalues and experimental energy levels leads to relatively larger disagreements in resonance position and, more seriously, to the interchange of resonances. This precludes using a simple shifting of wavelength scale. However, the resonances arise in different Green's functions, and can be shifted by using different ground-state ionization energies in the different Green's functions. Alternatively, one can retain a finite sum in relating the infinite sum to a Green's function, and use the finite sum to shift the resonances.

The model Green's-function technique is applicable to any element for which the multiphoton matrix element can be formulated in terms of a one-electron Green's function. The calculations presented here are for the alkali metals and the He metastable levels. For these elements there exists experimental data, and calculations using both truncated basis sets and the quantum-defect method. For two-photon ionization in the alkali metals, my calculations are in excellent agreement with those of Mizuno[28] for Li and Na, in agreement to a factor of three with Mizuno[28] for K, and in reasonable agreement with Lambropoulos and Teague[31,33] for Rb and Cs. For three-photon ionization my calculations are in excellent agreement with the measurements reported by Isenor[30] for K, Rb, and Cs at 6944 Å, while for Na my calculation is a factor of five smaller than the measurement reported by Isenor.[30] My calculations, as well as those of others, for two-photon ionization of Cs, are in good agreement with the recent measurements of Morellec *et al.*[40] but as much as two orders of magnitude lower than the measurements of Granneman and Van der Wiel.[34]

For three-photon ionization of helium my calculation for $(1s)(2s)^1S$ is in good agreement with the quantum-defect calculation of Olsen *et al.*[25] near the 6*s* resonance, but is considerably above the truncated basis set calculation of Olsen *et al.* In addition near 6950 Å my ^3S cross section is at least an order of magnitude larger than the calculation of Olsen *et al.*, which is in reasonable agreement with a recent measurement.[27] In summary, the model Green's-function calculations agrees reasonably well with other calculations and the measurements of Ref. 30 on the alkali metals. The model Green's-function technique is currently being applied to more complex atoms.

ACKNOWLEDGMENT

This work was supported by the U. S. Department of Energy.

[1]R. D. Hudson and L. J. Kieffer, At. Data 2, 205 (1971).
[2]C. Grey Morgan, Rep. Prog. Phys. 38, 621 (1975); Phys. Lett. 36, 1296 (1976).
[3]R. P. Madden and K. Codling, Phys. Rev. Lett. 10, 516 (1963).
[4]P. Esherick, J. A. Armstrong, R. W. Dreyfus, and J. J. Wynne, Phys. Lett. 36, 1296 (1976).
[5]M. Stobbe, Ann. Phys. (Leipzig) 7, 661 (1930); H. Hall, Rev. Mod. Phys. 8, 358 (1936).
[6]Y. Gontier and M. Trahin, Phys. Rev. 172, 83 (1968).
[7]D. R. Bates and A. Damgaard, Philos. Trans. R. Soc. London Ser. A 242, 101 (1949); M. J. Seaton, Mon. Not. R. Astron. Soc. 118, 504 (1958); A. Burgess and M. J. Seaton, *ibid.* 120, 121 (1960).
[8]B. A. Zon, N. L. Manakov, and L. P. Rapoport, Dok. Akad. Navk. SSSR 188, 560 (1969) [Sov. Phys.—Dokl. 14, 904 (1970)]; Zh. Eksp. Teor. Fiz. 60, 1264 (1971) [Sov. Phys. —JETP 33, 683 (1971)]; *ibid.* 61, 968 (1971) [*ibid.* 34, 515 (1972)].
[9]J. W. Cooper, Phys. Rev. 128, 681 (1962).
[10]E. J. McGuire, Phys. Rev. 175, 20 (1968).
[11]D. J. Kennedy and S. T. Manson, Phys. Rev. A 5, 227 (1972).
[12]M. Ya. Amusia, N. A. Cherepkov, and L. V. Chernysheva, Zh. Eksp. Teor. Fiz. 60, 160 (1971) [Sov. Phys.—JETP 33, 90 (1971)].
[13]J. S. Bakos, Adv. Electron. Electron Phys. 36, 57 (1974).
[14]P. Lambropoulos, in *Advances in Atomic and Molecular Physics*, edited by D. R. Bates and B. Bederson (Academic, New York, 1976), Vol. 12.
[15]R. A. Mapleton, Phys. Rev. 117, 479 (1960); J. Math. Phys. 2, 478 (1961).
[16]F. Herman and S. Skillman, *Atomic Structure Calculations* (Prentice-Hall, Englewood Cliffs, New Jersey, 1963).
[17]L. J. Slater, *Confluent Hypergeometric Functions* (Cambridge University Press, London, 1960).
[18]E. J. McGuire, Phys. Rev. A 3, 267 (1971).
[19]B. L. Beers and L. Armstrong, Jr., Phys. Rev. A 12, 2447 (1975).
[20]J. D. Jackson, *Classical Electrodynamics* (Wiley, New York, 1967).
[21]D. R. Hartree, Proc. Cambridge Philos. Soc. 24, 426 (1928).
[22]C. E. Moore, *Atomic Energy Levels*, NBS Circular No. 467 (U.S. GPO, Washington, D.C., 1949).
[23]J. B. Mann, Los Alamos Scientific Laboratory Report No. LASL-3960, 1967 (unpublished).
[24]N. L. Manakov, M. A. Preobragensky, and L. P. Rapoport, *Proceedings of the Eleventh International Conference on Phenomena in Ionized Gases, Prague, Czechoslovakia, 1974,* edited by I. Stolli (Czech. Acad. of Sci., Prague, Czech., 1974).
[25]T. Olsen, P. Lambropoulos, S. E. Wheatley, and S. P. Rountree, J. Phys. B 11, 4167 (1978).

[26]J. Bakos, N. B. Delone, A. Kiss, N. L. Manakov, and M. L. Nagaeva, Zh. Eksp. Teor. Fiz. 71, 511 (1976) [Sov. Phys.—JETP 44, 268 (1976)].
[27]L. A. Lompré, G. Mainfray, B. Mathieu, G. Watel, M. Aymar, and M. Crance, J. Phys. B 13, 1799 (1980).
[28]J. Mizuno, J. Phys. B 6, 314 (1973).
[29]G. A. Delone, N. L. Manakov, M. A. Preobrazhenskii, and L. P. Rapoport, Zh. Eksp. Teor. Fiz. 70, 1234 (1976) [Sov. Phys.—JETP 43, 642 (1977)].
[30]N. R. Isenor, in *Multiphoton Processes*, edited by J. H. Eberly and P. Lambropoulos (Wiley, New York, 1978).
[31]M. R. Teague and P. Lambropoulos, Phys. Lett. A 56, 285 (1976).
[32]M. R. Teague and P. Lambropoulos, J. Phys. B 9, 1251 (1976).
[33]P. Lambropoulos and M. R. Teague, J. Phys. B 9, 587 (1976).
[34]E. H. A. Granneman and M. J. Van der Wiel, J. Phys. B 8, 1617 (1975).
[35]M. Klewer, M. J. M. Beerlage, E. H. A. Granneman, and M. J. Van der Wiel, J. Phys. B 10, L243 (1977).
[36]M. R. Teague, P. Lambropoulos, D. Goodmanson, and D. W. Norcross, Phys. Rev. A 14, 1057 (1976).
[37]A. Rachman, G. La Planche, and M. Jaouen, Phys. Lett. A 68, 433 (1978).
[38]L. Armstrong, Jr. and J. H. Eberly, J. Phys. B 12, L291 (1979).
[39]D. Normand and J. Morellec, J. Phys. B 13, 1551 (1980).
[40]J. Morellec, D. Normand, G. Mainfray, and C. Manus, Phys. Rev. Lett. 44, 1394 (1980).